Chapter 12

Ultra-High Speed Data Relay Systems

Ricardo Barrios[1], Balazs Matuz[1] and Ramon Mata-Calvo[1]

12.1 Abstract

The *SpaceDataHighway*, the first operational service of high-speed data relay system based on optical inter-satellite links, has set a new milestone in space optical communications. Data relay systems are becoming crucial in applications such as Earth observation, where huge amounts of data need to be sent to Earth reliably and with low latency.

Optical communications plays a major role in such high-speed applications, since no-regulations are needed, because the lack of interference among users, and the huge amount of available bandwidth. Since the end of the 1990's, several experiments have shown the feasibility of such technology with several demonstrations from LEO, GEO and the Moon. The current state-of-the-art relay system architecture involves LEO and GEO satellites with optical inter-satellite links, and direct Ka-Band RF links from GEO to the Earth. Next generation systems may involve also UAVs, and may rely only on optical communications to exploit the full potential of these frequencies.

The main challenges of using optical links are the turbulence effects, when the link traverses the Earth's atmosphere, and the degrading impact of platform micro-vibrations because of the inherently small divergence of the transmitted beam. Such aspects have to be taken into account when designing future systems.

Together with the modulation, the forward error correction (FEC) defines the communications performance of the system. Following CCSDS coding recommendations, the performance of several coding schemes is analyzed; concretely Reed-Solomon codes, convolutional codes, turbo codes and low-density parity check codes are taken into account. One of the main characteristics of the atmospheric channel is the correlation of fading events, which requires further data protection to compensate for erasure events. Interleaving and packet level coding in combination with FEC are compared through simulations.

Finally, different approaches for data correction are considered. The complexity on board the GEO satellite can specially limit the use of the most advanced decoding schemes and data-protection for the upcoming generations of relay systems. The trade-off between performance and complexity is crucial in order to allow further system enhancements in terms of capacity, without endangering the whole system availability.

[1] German Aerospace Center (DLR), Satellite Networks Department, 82234 Wessling, Germany

This Chapter was originally published in: R. Barrios, B. Matuz and R. Mata-Calvo, "Ultra-high-speed data relay systems". In: S. K. Sharma, S. Chatzinotas and P. Arapoglou, [*Satellite communications in the 5G era,*]. London: The Institution of Engineering and Technology (IET), 2018, pp. 341-373.

12.2 Introduction

Data transfer from low Earth orbit (LEO) or pseudo-satellites to the ground is crucial for several applications where security is fundamental and where large amounts of data need to be transmitted. Perhaps, the most prominent example is the Earth observation missions.

A relay system based on geostationary equatorial orbit (GEO) satellites has two big advantages. First, it can provide coverage to the whole Earth surface with few relay satellites. Second, it increases the data-transfer availability of the terminals at LEO or on pseudo-satellites. In addition, a system based on free-space optical communications satisfies both security and high-data rates requirements. Data transmissions from hundreds of megabit per second to several terabits per second are possible, allowing expanding the optical network into space.

Since November 2016, the first operational high-speed data relay system is offering the *SpaceDataHighway* service, transferring data from LEO satellites to the ground via the European Data Relay System (EDRS) GEO satellites [1], [2]. High data-rate optical links are able to transfer data between satellites and a Ka-Band link relays the data to the ground.

A further development of this relay system, or the development of new ones, requires a detailed analysis of the physical layer, optimizing the system architecture by defining the optimal modulation formats, coding and data processing scheme, taking into account the platform limitations and channel impairments, while maximizing the data throughput.

The objective of this chapter is to define and analyze the key elements in the design of future ultra-high speed relay systems based on optical technologies.

12.3 Relevant missions and demos

Since end of the nineties, several optical communication terminals have been developed for LEO, GEO and Moon missions. Figure 12-1 summarizes the main missions related to optical communications, past and planed ones. The missions performing relay communications are highlighted in orange. In the upper part of Figure 12-1, there are the missions for GEO (SILEX, AlphaSat-LCT, EDRS, and LCRD) and Moon (LLCD). The LCRD is currently in development and it is planned for lunch in 2018. All of them are commented in the following sections. In the lower part of Figure 12-1, there are the missions for LEO payloads. The OPALS, SOTA and OSIRIS projects are focused in direct downlinks to Earth and they will not be further commented hereafter. In the future, for the SOTA mission is also planned links to aircraft and satellites [3].

Inter-satellite links were the framework of the SILEX project with two main objectives: to demonstrate the feasibility and performance of inter-satellite links and to relay video data from a LEO satellite to a ground station. The experiments involved two satellites that hosted the optical terminals: the ARTEMIS GEO satellite and the SPOT-4 LEO satellite. SPOT4, developed by Matra Marconi Space for CNES, was successfully launched in 1998 and ARTEMIS, developed by Alenia for the European Space Agency (ESA), in 2001 [4]. The laser terminals were developed based on intensity modulation (50 Mb/s with on-off keying (OOK) with no return to zero (NRZ) for the forward link) and direct detection of laser beams in the 800 nm range, allowing 50 Mbps data rate transmission. Since November 2001

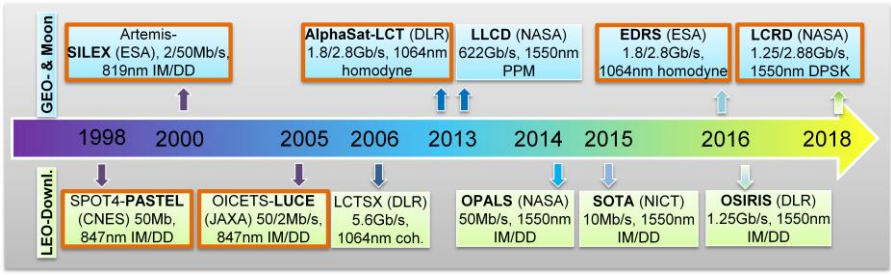

Figure 12-1: Timeline of optical terminals in space.

bidirectional links were performed between ARTEMIS and the ESA Optical Ground Station (OGS) at Canary Islands, Spain [5].

Other inter-satellite links were performed between ARTEMIS and OICETS satellites by JAXA and ESA since 2005, when the first bidirectional inter-satellite link took place. OICETS performed the return link at 2 Mb/s with 2-PPM. An avalanche photo-diode was used as receiver [6].

After the experience of SILEX, LEO inter-satellite communications based on coherent communications were the next step. The TerraSAR-X hosted the first coherent communications terminal in LEO based on this communications technology. The terminal implements binary phase shift keying (BPSK) modulation and homodyne detection using an optical phase-locked loop (OPLL). The terminal was developed by TESAT-Spacecom under DLR funding [7]. The counter-partner was installed on the NFIRE satellite that was developed by the USA department of Defense. Homodyne BPSK at 5.625 Gbps was performed between both satellites over distances up to 4900 km [8].

The European data-relay system—in operation since November 2015—relays data between LEO satellites to ground through a constellation of GEO satellites, and it will also support unmanned aerial vehicles (UAV) and aircrafts. After Alphasat and EDRS-A were launched, the first satellite constellation was already in orbit. On the GEOs, the laser communication terminal (LCT) is part of a hybrid optical-RF payload for data relay [9]. The LCT is serving as input section for RF payloads that have different capabilities regarding the programs: In the Alphasat mission, the data output of the LCT is directly connected to a 600 Mbit/s Ka-band modulator (transparent connection); while in the EDRS mission the data output of the LCT is subject to framing, encrypting and channel coding. Due to the resulting overhead, the data volume is increased and dumped through various Ka-band channels, each with 600 Mbps data rate. The ground segment performs decoding, decryption and de-framing.

It is noteworthy that recently, NASA successfully demonstrated bidirectional links with the optical terminal—based on 1500 nm systems—on board the Lunar Atmospheric Dust and Environment Explorer (LADEE), with a series of ground-space optical links demonstrations [10–12]. Using the Lunar Lasercom Space Terminal (LLST) payload in LADEE with maximum uplink and downlink rates of 20 and 622 Mbps, respectively [12]. The downlink operates with a 16-PPM modulation format, while the uplink does with a 4-PPM modulation.

The Laser Communications Relay Demonstration (LCRD) mission is currently under development by NASA, to serve as a testbed for different technologies and concepts required in a data relay system based on optical communications. LCRD will operate for a minimum of 2 years, with a terminal in GEO orbit hosting two optical communications modules, allowing for testing handover protocols between

ground stations. The main goals to be demonstrated in this mission are high rate bi-directional communications between ground and GEO, and to understand the feasibility of pulse-position modulation (PPM) for deep space communication—or other power-limited systems—or differential PSK (DPSK) for near Earth high data rate communications. Moreover, the LCRD will specifically target the study performance testing and demonstrations of coding, link layer, and network layer protocols over optical links [13].

12.4 System architectures

At the top of Figure 12-2, there is a depiction of the relay scenarios considered hereafter. The data relay system architecture consists of a user (U) terminal node, a data relay (R) node and a ground (G) station node. In this system architecture, there are two links, namely the user link and the feeder link. The U-R link is defined as the link between the user terminal node and the data relay node, while the feeder R-G link is defined between the data relay node and the ground station. The user terminal node can be a LEO (L) satellite or an UAV (X) and the data relay terminal is a GEO satellite. The ground station node can be, in principle, either optical or RF, accordingly to the desired Feeder-link technology. At the bottom of Figure 12-2, an abstraction of such communication chain is also provided, where both the U-R and R-G channel are responsible for degrading the transmitted information, resulting in errors in the data transmission.

Among all considered schemes, full decoding on board of the relay offers the best tradeoff between power, bandwidth and achievable error rate. From a channel coding perspective, the different communication links are considered independent, and the errors are recovered locally at the satellite, as well as on ground. This can be achieved by protecting the data stream over the U-R link via a forward error correcting code and decoding the data stream at the GEO relay. By doing so, the redundancy introduced at the user terminal to cope with U-R link errors is removed at the relay, and upon proper dimensioning of the channel code virtually all errors are corrected. Therefore, the encoded information sent by the user terminal via U-R link is decoded and reconstructed at the GEO relay prior to transmission over the R-G link. The redundancy introduced over this link is exploited to cope with the errors affecting the R-G link. This approach, although optimal in the sense of minimizing the amount of redundancy over the two links—hence, maximizing the spectral efficiency of the system—has the major drawback of requiring decoding of at the GEO relay. The provision of a (quasi) error-free decoding of information at the relay may require, in fact, the use of a powerful error correcting code over the U-R link with a complex decoder at the relay.[2] Therefore, various other options are discussed shifting decoding complexity from the relay to ground. Note also that the channel codes for the U-R link need to be fixed in advance, making later changes difficult. Other schemes, such as layered decoding offer more flexibility, since no decoding at the relay is performed.

[2] Note that the definition of complexity is very vague and changes in time. At the time being, existing relay systems barely implement channel coding mechanisms (exceptions are simple repetition codes). Therefore, also with regard to the high user data rates in the order of Gbit/s, decoding of modern codes at the relay is assumed to be impractical in the mid-term.

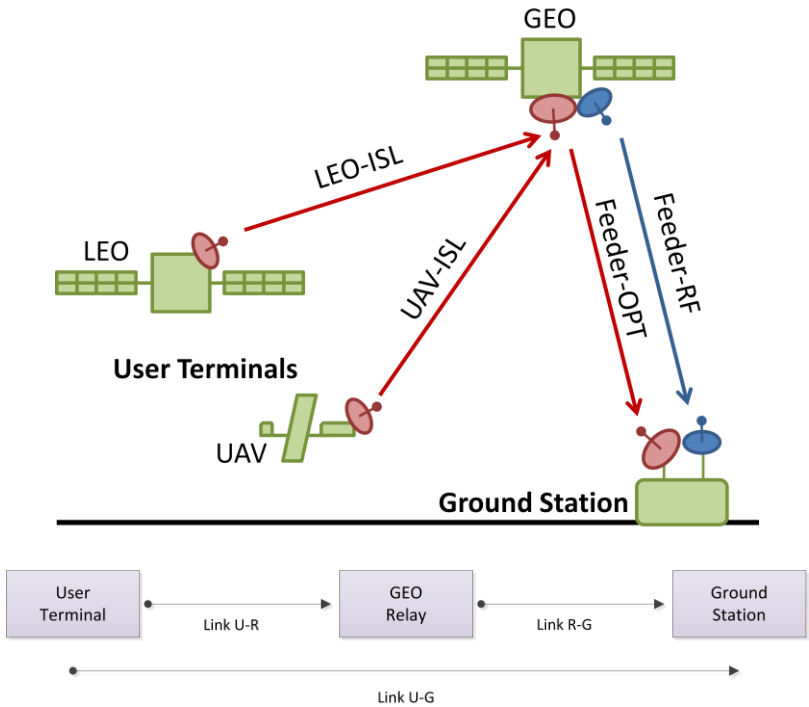

Figure 12-2: (Top) Scenarios for a GEO based relay system, and (bottom) abstraction of the communication channel.

To avoid implementing complex decoding algorithms at the relay, one may perform encoding at the user, route the data through the relay and perform all decoding operations on ground only. This scheme does not impose a strong complexity burden on the relay and provides some flexibility to change/update the physical layer (PHY) forward error correction (FEC) scheme independent of the relay. In particular, for the U-R link—where medium/low code rates are required—this solution lacks spectral efficiency.

FEC coding termination options

- **Full decoding on board the GEO:** FEC coding is applied independently in each link (optical ISL and optical feeder link). The GEO has to correct errors in the ISL channel and this may constraint the type and level of coding that can be applied, since resources on board the GEO are limited.
- **Decoding on ground only:** FEC coding is done, treating both the U-R and R-G links together. In this case, the GEO data relay does not perform any decoding. The ground station has then to correct errors occurred in both channels.
- **Partial decoding:** This scheme assumes that only some low-complexity decoding operations take place at the satellite. Another decoding step is done on ground where more decoding complexity is affordable.
  - **Layered coding:** this scheme implies that the user data is protected by an additional error correcting code on top of the physical layer code. This code is not decoded on the relay, but only on ground, thereby, shifting the decoding complexity to the receiver.

An alternative is to allow some low-complexity decoding operations on board of the relay. To improve the spectral efficiency, one may recover as many errors as possible at the GEO relay, with the given complexity constraint. Hence, from a spectral efficiency viewpoint, the best possible error control scheme that fits with the complexity limitations at the relay shall be used to protect the U-R link. On ground, a further decoding attempt is made to correct the remaining errors. Hereafter this approach is referred as partial decoding.

This approach is used in EDRS, where the U-R link is protected by a line product code, while the end-to-end FEC is based on a (255, 239) Reed-Solomon code [14]. The repetition code works at the very low end of the complexity scale providing, however, no coding gain. Options to render the U-R link more reliable can be based on more complex but still very light in computational burden error correction mechanisms.

Another approach is based on layered decoding. In particular, when the U-R link is subject to severe error events, e.g., due to strong pointing jitter, an additional channel code can be added on top of the low-complexity PHY FEC scheme. In the following, this code is referred to as packet level (PKT) code or erasure code. In this case, at the GEO only the weak PHY code is decoded, correcting some errors on the U-R link. A mandatory error detection mechanism marks each PHY codeword either as correct or erroneous. All erroneous data is discarded. The remaining data, after some processing is encoded and transmitted to the ground where after correcting the errors on the R-G link the PKT decoder attempts to recover the erroneous data from the U-R link—i.e. those not recovered at the GEO relay. Upon a proper design, high spectral efficiencies can be reached here with some penalty in performance with respect to full decoding on board of the satellite.

12.5 Optical channel model

12.5.1 *Atmospheric channel*

The atmospheric turbulence can be defined by the strength of the fluctuations in the refractive index, represented with the refractive-index structure parameter C_n^2 with units of $m^{-2/3}$. Hereafter, for all required calculations, the well-known Hufnagel-Valley vertical profile is used [15]. The intensity of the received signal (for both coherent and non-coherent modulations) is affected by fading, resulting in time-varying detected power, due to scintillation and beam-wander. Scintillation is the result of self-interference processes due to phase distortions and beam-wander are atmospheric induced pointing errors. The former is defined by the scintillation index (SI)—i.e. the normalized variance of the received optical power—and the latter by the RMS value of the beam displacement. Expressions to calculate the SI are readily available elsewhere [15].

The intensity can be modelled as a random variable governed by a lognormal probability density function (PDF) in the case of weak turbulence regime for a point receiver and works well in all regimes of turbulence for aperture averaged data [16], [17]. A process for the generation of lognormally correlated time samples has been presented elsewhere [18]. Additionally, the lognormal channel attenuation can be modelled as low pass process with a characteristic frequency—that depends on the atmospheric turbulence strength and the speed of the different turbulence layers—having -8/3 and -17/3 power law slope for low and high frequencies, respectively [19]. The cut off frequency characterizing the coherence time of

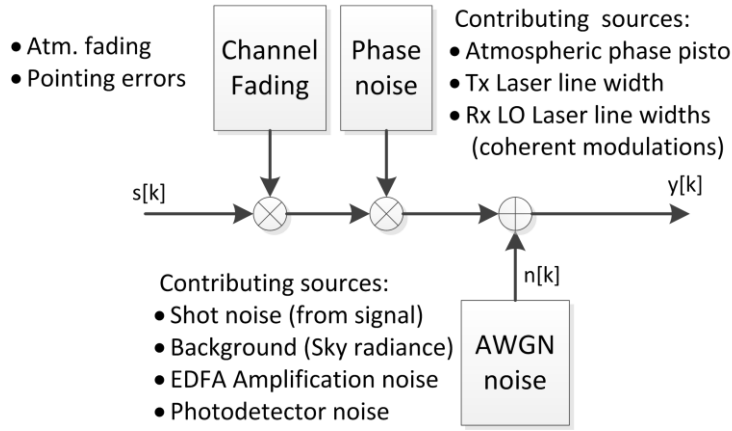

Figure 12-3: General block diagram of the channel model after the photodetector.

the atmosphere is known as the Greenwood frequency [20]. The scale of the atmospheric coherence time, i.e. the inverse of the Greenwood frequency, is usually in the order of tens of milliseconds.

The block diagram, shown in Figure 12-3, describes a general channel model including all the channel impairment effects due to turbulence and pointing errors due to terminal micro-vibrations.

Once the basic scenarios are defined in Section 12.4 above, some calculation of the relevant parameters of the optical channel can be done in order to set the operational constrains of the different links. It is noteworthy that the L-R link is not affected by turbulence and, thus, the parameters related to atmospheric turbulence are calculated only for the X-R and R-G links.

The Fried parameter r_0 measures the integrated turbulence strength along a given propagation path, and is given by

$$r_0 = \left(0.423k^2 \sec\zeta \int_{h_0}^{H} C_n^2(h)\, dh\right)^{-3/5}, \tag{12.1}$$

where $k = 2\pi/\lambda$ is the wavenumber, with λ being the wavelength, and ζ is the elevation angle.

The higher the value of the Fried parameter is, the weaker the turbulence. Typical values for weak turbulence are in the range of tens of centimeters. In the X-R link the Fried parameter is about two orders of magnitude larger than the typical values for weak turbulence, indicating that little to no influence from turbulence should be present in such links.

Figure 12-4(a) presents an estimation of the beam wander effects over the X-R link. The angular beam wander, which represents the variance of the atmospheric induced pointing errors, can be calculated as [15]

$$\theta_{BW}^2 = 0.54 \left(\frac{\lambda}{2W_0}\right)^2 \left(\frac{2W_0}{r_0}\right)^{5/3}, \tag{12.2}$$

where W_0 is the beam radius at the transmitter output plane. Moreover, it can be readily seen that the beam wander loss, which can be estimated as $L_{BW} = \exp(-G_T\theta_{BW}^2)$ for a Gaussian profile, is negligible for the UAV-to-relay link. This is so mainly due to the fact the standard deviation of their angular variations is about two orders of magnitude lower than the UAV transmitter beam divergence, which is in the order of tens of microradians.

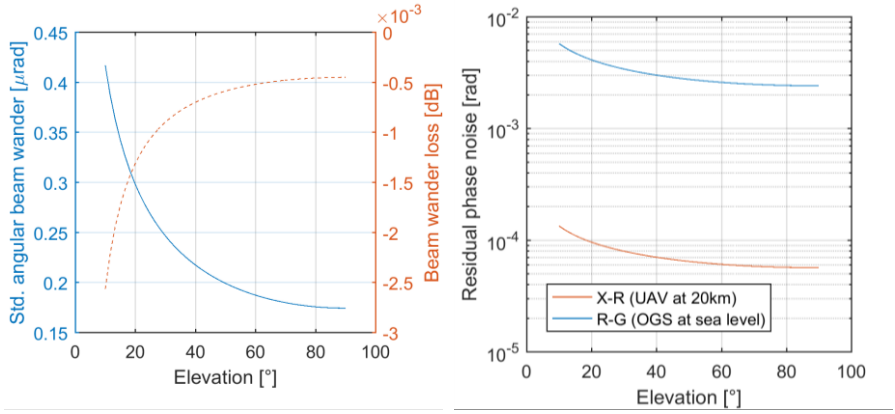

(a) (b)

Figure 12-4: (a) Angular beam wander and beam wander loss for the X-R link, and (b) residual phase noise error due to atmospheric piston of two different terminal altitudes and different elevation angles, for a direct link with GEO satellite.

The atmospheric turbulence of the optical channel produces intensity and phase fluctuations. The phase distortions, induced by atmospheric turbulence, produce time-of-arrival jitter on the receiver signal, which is negligible for non-coherent modulation formats. In the case of coherent modulation formats, the influence of the atmospheric piston can be modelled through its effect on the residual phase noise as [21]

$$\sigma_{\phi}^{2} = 1.328\left(\frac{v_{\perp}}{r_0}\right)^{5/3}\omega_n^{-5/3}, \tag{12.3}$$

where ω_n is the natural frequency of the receiver optical phase-locked loop (OPLL) and $v_{\perp}$ is the wind speed vertical profile normalized with respect to the C_n^2 profile, which can be calculated as shown elsewhere [21]. Figure 12-4(b) shows the residual phase noise due to atmospheric piston for the X-R and R-G links, with $\omega_n = 50$kHz, where it can be readily seen that values are always below 0.01 rad for all the analyzed conditions. It is already known that only values in the order of 0.1 rad or above can produce a significant deterioration of homodyne receivers [21]. Therefore, it is determined that atmospheric piston does not play a significant role—when the OPLL is optimally designed [22]—in the reception of optical coherent modulation formats, for the relay scenarios analyzed here.

Figure 12-5 presents the scintillation index value and the scintillation loss for the X-R and R-G links. The scintillation index gives a measure of the normalized standard deviation of the received optical intensity, and depends inversely on the link elevation angle, i.e., the lower the elevation the higher the scintillation index as a longer atmospheric path is traversed. When estimating the scintillation loss, a target availability of 99.6 % was assumed [23]. On the one hand, it can be seen that in the X-R link, for elevation angles above 15 °, the SI loss is less than 0.5 dB, indicating very weak turbulence. On the other hand, for the R-G link, for a 60 cm receiving telescope the SI loss could go as high as 2.5 dB for low elevation angles. Nevertheless, typical elevation angles in a GEO-ground scenario are above 35 °, where the SI loss would amount to approximately 1 dB or less. Because the SI value is always below 0.1, the atmospheric turbulence in all scenarios can be regarded to operate under a weak turbulence regime. The low values of SI are explained, as the propagation occurs only in the higher portion of the atmosphere for

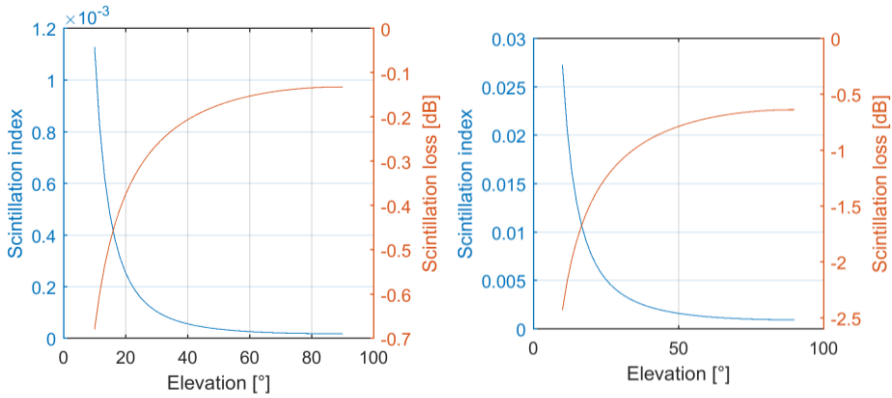

Figure 12-5: Scintillation index and scintillation loss for a direct link with a GEO satellite from (left) an UAV at 20 km, and to (right) an OGS (60 cm aperture) at sea level at different elevation angles. The target availability assumed was 99.6 %.

the X-R link case, where turbulence is the lowest. In the case of the R-G link, although the optical wave traverses the whole atmosphere, a fair amount of aperture averaging takes place effectively reducing the scintillation indes. The SI expressions for the uplink and downlink has been given elsewhere [15].

12.5.2 *Pointing errors and micro-vibrations*

Micro-vibrations of the transmitter platform contribute to the pointing errors and they can be modelled by a beta distribution, when the pointing bias is assumed to be zero. Therefore, the probability density function of the received optical power, due to only pointing errors, is given by [24]

$$f_I(I) = \beta I^{\beta-1}, \;\; 0 \le I \le 1, \;\; 0 < \beta < \infty. \tag{12.4}$$

where the parameter $\beta = W_0^2/(4\sigma_e^2)$ characterizes the random micro-vibrations of the user terminal; W_0 being the laser bean radius at the transmitter, and $\sigma_e = \left[\int \theta_e^2(f)df\right]^{1/2}$ is the root-mean-square (RMS) of the random jitter [25]. To complete the model, a power spectral density (PSD) of the user terminal vibrations must be assumed, in order to take into account the temporal behavior of the transmitting telescope pointing errors. In the past, the European Space Agency (ESA) proposed a model for the micro-vibrations PSD, for the optical communication payload SILEX, given by [26]

$$\theta_e^2(f) = \frac{2\sigma_e^2}{\pi(1 + (f/f_{e0})^2)}. \tag{12.5}$$

where f_{e0} is the cut-off frequency of the PSD. For the case of the ESA model, this frequency was set to 1 Hz to model a LEO platform. For an UAV, it could be expected that the PSD to be spread over a larger bandwidth, taken into account the influence of wind gusts.

As an estimation of the order of magnitude of the RMS random jitter σ_e, a quick overview of available literature shows that for LEO terminals σ_e is in the range of 20–45 μrad [25], and for an aircraft terminal few hundreds of microradians has been reported [27]. These figures refer to total amounts due to vibrations of the space- or aircraft, which are more relevant in the initial pointing and acquisition stages of the link, and usually compensated through a coarse pointing assembly.

For the communication stage of link, a fine pointing assembly—usually a fast steering mirror (FSM)—is most likely also part of the LCT that helps in further reducing the pointing errors. Nevertheless, there is always a residual pointing error, which is the relevant figure for the communications phase of the link. Values reported in the literature for the residual pointing errors (jitter) range from as low as 0.3 μrad [28] and 0.8–1.53 μrad [29], to as high as 2.6 μrad [30], for satellite platforms. In case of UAVs, for platforms flying altitudes of 10 km or above, reported residual pointing error jitters are in the order of some tens of micro radians [31].

To summarize, Table 12.1 presents a list of relevant parameter for all the scenarios defined, with some typical values for the sake of example. When the user terminal is a LEO satellite, the transmit power and aperture are changed to reflect the cases of a small and big LEO terminal. The small terminal has a 7 cm aperture with a 3 W power output, while for the big terminal a 15 cm aperture and a 5 W power output is assumed. In both cases, the transmitter laser is assumed collimated. For the UAV, 50 W transmitter power has been assumed, and 10 W for GEO platform.

On the one hand, it can be readily seen that for the X-R link, although it traverses the atmosphere, the atmospheric channel is quite benign due to the fact that only the upper part of the atmosphere plays a role. On the other hand, in case of the R-G link, although the whole atmosphere is within the propagation path of the downlink laser, a fair amount of aperture averaging takes place significantly reducing the effects of scintillation. This is due to the relatively large receiving aperture diameter at the ground station is 60 cm, when compared to typical values of the Fried parameter. Additionally, the atmospheric coherence time is about some tens of milliseconds, giving an indication of the interleaver size to cope with the

Table 12.1: Relevant link parameters for all analyzed links for an optical GEO based relay system. The links are LEO to Relay (L-R) for a small and big platform, UAV to Relay (X-R) and Relay to Ground (R-G).

Parameter	**Units**	**Small L–R**	**Big L–R**	**X–R**	**R–G**
Elevation	°	—	—	40.00	35.00
Link distance	km	40000.00	45000.00	35980.00	38394.12
Wavelength	nm	1550.00	1550.00	1550.00	1550.00
Fried parameter	cm	—	—	1612.71	13.94
Greenwood frequency	Hz	—	—	0.34	34.46
Atmospheric coherence	ms	—	—	2983.71	29.02
Res. pointing jitter	μrad	0.63	0.32	11.79	—
Coherence atm+jitter	μs	89.42	89.23	89.35	29020.00
Scintillation index		—	—	1.74E-04	1.36E-2
Tx Altitude	km	500.00	500.00	20.00	36000.00
Atmospheric attenuation	dB	—	—	-0.01	-0.50
Tx power	W	3.00	5.00	50.00	10.00
Tx Telescope diameter	cm	7.00	15.00	12.00	25.00
Tx Divergence	μrad	19.94	9.30	50.00	5.58
Rx Telescope diameter	cm	25.00	25.00	25.00	60.00

correlated fading events. Finally, the residual jitter and its coherence time—for the U-R channel—are calculated by simulating the platform pointing errors using the model in (12.5). Next, the half-width-half-maximum point of the channel state autocorrelation at the receiver plane was measured, assuming that the transmitter pointing mechanism can effectively reject vibration up to about 500 Hz, in the communication tracking phase of the link [32]. The total amount of initial jitter σ_e assumed was 20 and 45 μrad for the small and large LEO platform, with a PSD cut-off frequency f_{e0} of 1 Hz, following the ESA model [26]. For the UAV case, a σ_e of 100 μrad was assumed with $f_{e0} = 50$ Hz, to reflect the higher vibration regime due to the wind gust affecting the aircraft.

A special consideration is made for the X-R link, where the user is an UAV platform. Due to the strong residual pointing jitter, the divergence of the transmitter telescope is optimized to counter the pointing loss effects. The resulting optimum divergence is about 50 μrad. The UAV's telescope is selected to be 12 cm as this size falls within the requirements of the tracking system [33], [34]. Nevertheless, this aperture diameter has no impact in the link budget calculation on the X-R link, as the transmitter is assumed non-collimated and its gain is obtained through the divergence value.

12.5.3 *Light coupling efficiency*

In every receiver chain, collected light by the telescope must be coupled into a photoelectric converter device, which might be preceded by fiber waveguide stage as in an EDFA pre-amplified receiver chain case. When light needs to be coupled into a single mode fiber (SMF), the coupling efficiency under the presence of atmospheric turbulence is [35]

$$\eta_C = 8a^2 \int_0^1 \int_0^1 \exp\left[-\left(a^2 + \frac{D_R^2}{4\rho_0^2}\right)\right] I_0\left(\frac{D_R^2}{4\rho_0^2} x_1 x_2\right) dx_1 dx_2, \tag{12.6}$$

where $a = \pi D_R W_m/(2\lambda F)$, W_m is the field radius of the fundamental mode that propagates through the SMF (usually about 5 μm), F is the focal length of the receiving telescope, and $\rho_0 = 0.48 r_0$ is the atmospheric coherence radius—which is directly related to the Fried parameter give in (12.1).

In the uplink direction—i.e. for the UAV to GEO relay—the turbulent structures defined by ρ_0 are much larger than the probable size of the GEO satellite receiving aperture and thus $\rho_0 \gg D_R$. Consequently, the maximum fiber coupling efficiency $\eta_C = 0.815$ can be obtained, provided that the receiver telescope has optimize the ratio D_R/F such that $a = 1.12$ [36].

In the downlink direction, for the GEO relay to ground link, the D_R/ρ_0 ratio is larger than unity, indicating that some amount of wavefront distortion is capture by the receiving aperture. Therefore, the shape of the focused light can differ greatly from an Airy pattern, effectively producing additional coupling losses. In order to counterattack this phenomena, adaptive optics (AO) is often used to correct the incoming distorted wave, which can be decomposed into several orthogonal modes described by the Zernike polynomials [37]. To estimate the possible gain when applying AO techniques, a generalized Fried parameter $r_{0,N}$ can be estimated in terms of the number of Zernike modes N corrected as [38]

$$r_{0,N} = 0.286 r_0 \left(\frac{3.44}{C_N}\right) N^{-0.362}, \tag{12.7}$$

where C_N is the corresponding coefficient for the number of modes N being corrected as given by Noll [37].

Finally, in cases where the light is directly coupled over the photodetector, the diameter of the time-averaged (long-term) focal spot can be larger than the detector diameter. If the Fried-parameter r_0 is smaller than the aperture diameter D_R, the long-term intensity distribution $I(r)$ can be modelled as a Gaussian distribution with standard deviation $\sigma \approx 0.42\lambda F/r_0$. Integrating the intensity distribution over the area of the detector yields the encircled—i.e. the detectable—power.

12.6 Noise model

The calculation of the available signal-to-noise ratio (SNR) is essential when assessing a link performance. The symbol-level SNR is defined as

$$SNR = \frac{I_R^2}{\sigma_s^2 + \sigma_{\mathrm{B}}^2 + \sigma_{\mathrm{ASE}}^2 + \sigma_{\mathrm{s-ASE}}^2 + \sigma_{\mathrm{ASE-ASE}}^2 + \sigma_{\mathrm{LO\text{-}ASE}}^2 + R_I^2 \mathrm{NEP}^2 B_e^2}, \quad (12.8)$$

where R_I is the responsivity of the photodetector and $I_R = R_I P_R$ is the generated signal photocurrent, for a certain received optical power P_R. When the received signal is coherently modulated, and a local oscillator (LO) with optical power P_{LO} is used, then $I_R = 2R_I\sqrt{P_{\mathrm{LO}}P_R}$. Moreover, B_e is the electrical bandwidth of the photodetector or the subsequent low-pass electrical filter, which is chosen to match the required bandwidth for the specific symbol rate of the modulated received signal. In addition, the noise equivalent power (NEP) characterizes the noise figure of the photodetection process, which includes the effects of thermal and dark current noise.

The shot noise variance—product of the intrinsic quantum nature of the light—can be approximated by $\sigma_s^2 = 2qI_R MFB_e$; where q represents the elementary charge, M is the mean avalanche gain (higher than unity for APD photodiodes), and F is the excess noise factor. Similarly, the noise due to optical background power is calculated in the same manner.

The total background radiation can be characterized by the spectral radiance of the sky that depends on the elevation angle, and changes for day and night operation. In night time, the sky emissivity for a nearly horizontal path through the atmosphere is essentially that of a blackbody at the temperature of the lower atmosphere. The behavior for daytime conditions will be very similar to that of night time, with the corresponding change due to higher temperatures, and the addition of scattered sun radiation below 3 μm [39]. The background noise can be modeled as $\sigma_{\mathrm{B}}^2 = 2qR_I P_B MFB_e$, where $P_B = N_B B_o(\pi D_R \mathrm{FoV}/4)^2$ is the background optical power, which depends on the spectral radiance of the sky N_B, the receiver aperture D_R, optical filter bandwidth B_o and detector's field of view FoV.

Amplified spontaneous emission (ASE) noise is inherent property of the used optical amplifiers [40]. The power spectral density noise is assumed bilateral and for each component the complex noise variance can be written as $N_{0,ASE} = h\nu(G-1)n_{sp}/2$, where h is the Plank's constant, G is the amplifier gain and n_{sp} is the spontaneous emission factor, which is always greater than one. It is noteworthy that the variance depends on the frequency ν, showing that ASE is not really white because of this dependence with ν. However, for the normal bandwidth values required by data transmission systems, the ASE noise is considered flat and thus can be assumed as an AWGN process.

At the optical-to-electrical conversion stage, an ASE shot noise and two beat components are generated; along with the beating noise between the signal and the ASE $\sigma^2_{\mathrm{s-ASE}}$, and between the ASE with itself $\sigma^2_{\mathrm{ASE-ASE}}$. Assuming only one polarization, all are assumed AWGN and are given by [41]

$$\begin{aligned}\sigma^2_{\mathrm{ASE}} &= 2qN_{0,\mathrm{ASE}}B_oR_IB_e,\\ \sigma^2_{\mathrm{s-ASE}} &= 4I_RMFN_{0,ASE}R_IB_e,\\ \sigma^2_{\mathrm{ASE-ASE}} &= R_I^2N^2_{0,\mathrm{ASE}}B_e(2B_o-B_e).\end{aligned} \tag{12.9}$$

In the case of coherent detection, an extra beating noise term appears due to the interaction of the local oscillator power P_{LO} with the ASE component from the EDFA pre-amplifier in the receiver chain, which is given by $\sigma^2_{\mathrm{LO\text{-}ASE}} = 2R_I^2P_{\mathrm{LO}}N_{0,\mathrm{ASE}}B_e$ [42].

For the cases when an EDFA booster amplifier is used in the transmitter side, its ASE noise can be referred to the receiver chain as part of the background noise, in the form of an additional background optical power given by $P_{ASE-T_x} = 0.2hcG_TF_TD_T^2D_R^2/(R^2\lambda^3)$,where G_T and F_T refer to the booster amplifier gain and noise factor, respectively [41].

12.7 Link budget

The channel model includes several effects: the transmission losses, the atmospheric turbulence effects and the platform micro-vibrations. A simple way to see the different phenomenon affecting the optical link is through the expression of the received optical power P_R detected at distance L, which is given by

$$P_R = P_TG_T\eta_T\eta_{ATM}L_{FS}L_pL_{SI}G_R\eta_R\eta_C, \tag{12.10}$$

where P_T is the transmitted average optical power with wavelength λ, $G_T = (\pi D_T/\lambda)^2$ and $G_R = (\pi D_R/\lambda)^2$ are the transmitter and receiver gains, respectively; η_T and η_R are transmitter and receiver efficiencies, respectively, while η_{ATM} is the atmospheric attenuation; $L_{\mathrm{FS}} = (\lambda/4\pi L)^2$ is the free-space loss. From the terms in (12.10), G_T, G_R, η_T, η_R, η_{ATM} and L_{FS} are considered either static or slow-varying losses—respect to the time scale of the communication process—and do not have an impact on the statistical behavior of the fading process. Moreover, $L_p = \exp(-G_T\theta^2_{BW})$ corresponds to the pointing errors. Finally L_{SI} is the SI loss, respectively. The former can be calculated with a method from [43], and the latter with an expression from [23]

$$L_{SI} = \left(3.3 - 5.77\sqrt{\ln 1/p}\right)\sigma_I^{4/5}, \tag{12.11}$$

where σ_I^2 is the scintillation index, $p = 1 - \mathrm{av}$ is the fractional outage time, and av is the target availability, which in the scenario analyzed here is set to 99.6 %..

Finally, the telescope collected light must be coupled into a photodetector, which will exhibit a certain coupling efficiency η_C. When light needs to be coupled into a single mode fiber (SMF)—as in an EDFA pre-amplified receiver chain—the coupling efficiency under the presence of atmospheric turbulence, for the R-G link, is a function of the ratio of the receiver aperture diameter to the Fried's parameter D_R/r_0 [35]. For the downlink case, i.e. in the R-G link, it is assumed that 50 Zernike modes are corrected by applying AO correction. This represents an improvement of about 13 dB with respect to a system without AO, and about 7 dB with a system that compensates for the tip-tilt Zernike modes, i.e. corrects for angle-of-arrival fluctuations.

In the uplink direction, i.e. for the U-R link, the transversal coherence of the wave is much larger than the probable size of the GEO receiving telescope aperture. Consequently, the maximum fiber coupling efficiency $\eta_C = 0.815$ can be obtained.

In order to carry out the link budget calculations, some assumptions on the transmitter and receiver chain have to be made. In the transmitter, the booster amplifier is assumed to work on a regime with a 45 dB gain and a 6 dB noise figure. These parameters are necessary in calculating the effect on the transmitter booster ASE noise, which is effectively included as an extra background power level.

For the receiver chain, it is assumed that an optical filter of 0.8 nm—i.e. corresponding to a dense wavelength division multiplexing (DWDM) grid of 100 GHz—is present, which is a well-known standard assumption for 1550 nm. The receiver optical chain has a pre-amplifier with 30 dB of gain, with 4 dB noise figure. The pre-amplifier is assumed to be used in both coherent and non-coherent reception, thus, the light coupling power loss always refers to fiber coupling efficiency. The photodetector is a PIN diode with a maximum 20 GHz electrical bandwidth, 0.75 A/W responsivity, and a noise equivalent power NEP=2.5 pW/$\sqrt{\text{Hz}}$. In addition, for the case of coherent detection a 10 dBm LO laser is considered.

It is noteworthy that, in the optical domain, data rates up to 40 Gbit/s are achievable with current technology using a single optical channel. Modulator and receivers for 40 Gbit/s are also available. However, currently for data rates beyond 25 Gbit/s usually wavelength division multiplexing (WDM) techniques are taken into consideration. In fiber communications it is a well-known technique that leads to the ITU recommendations G.694.1 and G694.2 for dense WDM (DWDM) and course WDM (CWDM) spectral grids, respectively. Such recommendations fix the

Table 12.2: Link budget calculation for all link scenarios defined by Table 12.1.

Parameter	**Units**	**Small L–R**	**Big L–R**	**X–R**	**R–G**
Tx power	dBm	34.77	36.99	47.00	40.00
Tx antenna gain	dB	102.15	108.77	95.05	113.20
Tx antenna efficiency	dB	-3.01	-3.01	-3.01	-3.01
Tx pointing loss	dB	-0.06	-0.15	-1.68	0.00
Free-space loss	dB	-290.22	-291.24	-289.30	-289.86
Atmospheric attenuation	dB	0.00	0.00	-0.01	-0.50
Scintillation loss	dB	0.00	0.00	-0.32	-1.84
Link margin	dB	-1.00	-1.00	-1.00	-3.00
Rx antenna gain	dB	114.10	114.10	114.10	120.88
Rx antenna efficiency	dB	-3.01	-3.01	-3.01	-3.01
Rx light coupling loss	dB	-0.89	-0.89	-0.89	-14.72
Total link loss	dB	-82.02	-76.44	-90.07	-81.00
Total Rx power	dBm	-47.24	-39.45	-43.08	-41.00
Total equivalent background power	dBm	-80.92	-74.75	-74.65	-69.24

central frequencies of the transmitter laser and the optical channels for the multiplexers and de-multiplexers. This technology is however usually limited to wavelengths in the range of optical C-Band and L-Band for DWDM and in the range between 1270 and 1610 nm for CWDM.

Table 12.2 presents the link budget calculation for all the scenarios selected. In the U-R link, the user can be either an UAV or a LEO satellite—that can be a small or big platform. The bottom row gives the equivalent background noise power seen by the receiver photodetector, i.e. after the pre-amplifier, and includes the transmitter booster ASE noise and the sky irradiance background noise.

Based on the total received power calculated in the link budget presented in Table 12.2, a calculation of the photons per bit (PPB) at different bit rates can be performed.

$$\mathrm{PPB} = \frac{P_R}{E_\lambda R_b}, \tag{12.12}$$

where R_b is the uncoded data bit rate and $E_\lambda = hc/\lambda$ is the photon energy; with h being the Planck's constant and c is the speed of light in vacuum.

The PPB metric is useful for providing a first idea on the maximum bit rates that in principle could be achieved with an optically pre-amplified receiver. In Ref. [44], a rather complete table presents a list of high-sensitivity optical receiver demonstrations. There, previously reported sensitivities for uncoded transmission are in order of 147 PPB for OOK at 10 Gbps, 45 PPB for DPSK at 12.5 Gbps, and some 100 PPB for BPSK at 10 Gbps [44]. Hereafter, the assumption is made that for data rates in the order of few tens of Gbit/s—in a timeframe of about 10 years from now—on-going developments could potentially allow for receiver sensitivities close to 50 PPB, for coherent modulations and DPSK, and about 100 PPB for OOK.

The estimation of the PPB for each link at 0.1, 1, 5, 10 and 20 Gbps is presented in Table 12.3. By inspecting the calculated values, it is readily seen that for a small LEO platform to the GEO relay data transmission using OOK would be possible for data rate below the Gbit/s regime, and to transmit about 1 Gbps or more then DPSK or BPSK modulation would be required. In the case of a big LEO platform, transmission up to 10 Gbps seems to be possible. When the user communicating with the GEO relay is an UAV, data rates up to 5 Gbps would be feasible using either DPSK or BPSK, while OOK could work up to a few Gbit/s. Finally, in the downlink from the GEO relay to the OGS, data rates up to 10 Gbps could be possible, while for higher rates it would be advisable to split the total throughput into various channels using WDM techniques.

Table 12.3: Average received photons per bit, for all link scenarios defined by Table 12.1 and Table 12.2. The received average power is taken from Table 12.2

Bit rate	Small L–R	Big L–R	X–R	R–G
100 Mbps	1470.09	8837.77	3831.27	6182.63
1 Gbps	147.01	883.78	383.13	618.26
5 Gbps	29.40	176.76	76.63	123.65
10 Gbps	14.70	88.38	38.31	61.83
20 Gbps	7.35	44.19	19.16	30.91

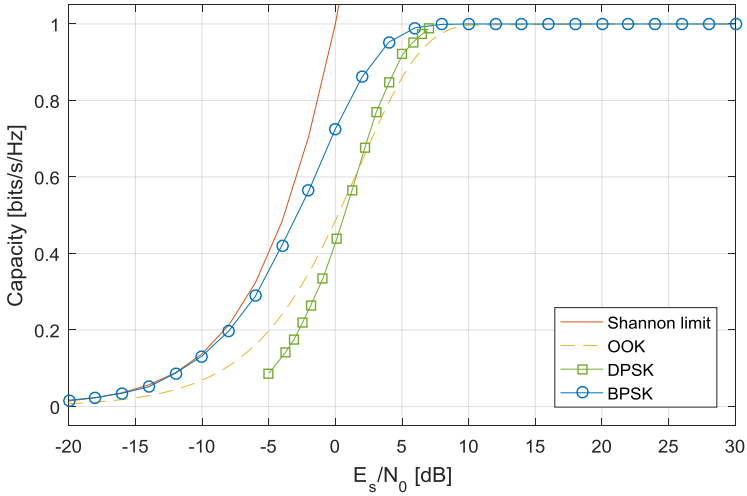

Figure 12-6: Maximum capacity as a function of the symbol-level SNR, for different modulation formats. The plot for DPSK corresponds to the performance when the observation window comprises two symbols. The curve for DPSK was taken from [45].[3]

Finally, the channel capacity for a given symbol-level SNR, for different modulation formats, is presented in Figure 12-6. The plot for DPSK corresponds to the performance when the observation window comprises two symbols [45]. Note that multi-symbol detectors may close the gap with respect to the BPSK capacity curve. To make use of this information, the calculation of the available SNR for all links is presented in Table 12.4. Values given are for OOK modulation format. In addition, values for DPSK and BPSK are given in square brackets and parenthesis, respectively. Moreover, only values for which reliable communication is possible—in terms of the receiver sensitivity discussion presented above—are given. It is noteworthy to mention that SNR values presented in Table 12.4 are based on the link budgets give in Table 12.2, where the transmitter is assumed to be average

Table 12.4: Average symbol-level SNR in decibels, for all link scenarios defined by Table 12.1 and Table 12.2. Values presented are for direct detection, i.e. OOK and DPSK (in square brackets), and for coherent detection, i.e. BPSK (in parenthesis). SNR values are not given for bit rates at which pre-amplified receiver sensitivity is not enough to allow reliable communication.

Bit rate	Small L–R	Big L–R	X–R	R–G
100 Mbps	22.3 [22.0] (24.6)	33.1 [31.9] (32.3)	28.4 [27.6] (28.8)	31.2 [30.1] (30.7)
1 Gbps	12.3 [12.0] (14.6)	23.2 [21.9] (22.3)	18.4 [17.6] (18.8)	21.2 [20.1] (20.7)
5 Gbps	—	16.2 [15.0] (15.3)	11.4 [10.6] (11.7)	14.2 [13.1] (13.8)
10 Gbps	—	13.2 [12.0] (12.3)	—	11.2 [10.1] (10.8)
20 Gbps	—	—	—	—

[3] The curve for DPSK shown here is correctly plotted. In the original publication the DPSK curve is wrongly plotted.

power limited. Thus, the transmitted peak power for OOK is twice the average, while for DPSK and BPSK the peak and average power are the same. Note that, although they assume the same average power, the SNR value for BPSK is larger than for DPSK, reflecting the fact that former uses coherent detection using a laser local oscillator.

When compared with the maximum achievable capacity curve in Figure 12-6, the expected SNR values indicate that, in principle, maximum profit of the channel usage could be obtained. In this scenario, error correction with high code rates can be applied in order to maximize the bandwidth occupancy for the transmission of information bits.

Up to this point, all analysis has been performed considering uncoded transmission only. Nevertheless, a communications system will always be protected with an error correction code. In the following section, the implementation of forward error correction (FEC) codes is presented, while taking into account the particularities of the user and feeder optical channels in a GEO relay scenario as well as the type of processing.

12.8 Forward error correction

An overview of different FEC codes defined in the framework of the Consultative Committee for Space Data Systems (CCSDS) for near earth and deep space communications is provided in the following. These codes that were intended for point-to-point links, i.e., without relay, can be used as building blocks for data relay systems. Complete solutions for data relay systems will be discussed in the next subsections. Amongst others, the following channel codes are defined in CCSDS [46][47][48].

- **Reed-Solomon (RS) codes**. Hard decision decoding is done for short/medium sized blocks [49]. Due to the limited block length and the fact that soft information is not exploited at the decoder, coding gain is limited, in particular w.r.t. modern, iterative codes.
- **Reed-Solomon and convolutional codes (RS+CC)**. This serially concatenated scheme consists of an inner convolutional code processing soft information and an outer RS code fixing residual (bursty) symbol errors of the inner code. Due to the lack of iterating between the blocks and relying on soft-input hard-output inner decoders, this option is inferior to modern codes in terms of performance.
- **Turbo codes.** Both serial concatenated convolutional codes (SCCCs) and parallel concatenated convolution codes (PCCCs) are proposed in the CCSDS standard and belong to the class of iteratively decodable turbo codes with excellent performance.
- **Low-density parity check (LDPC) codes**. Different types of LDPC codes are part of CCSDS. Some of them and originate from the Digital Video Broadcasting – Satellite 2 (DVB-S2) standard. Thanks to the large block lengths and soft decoders, LDPC codes belong to one of the most powerful coding schemes.

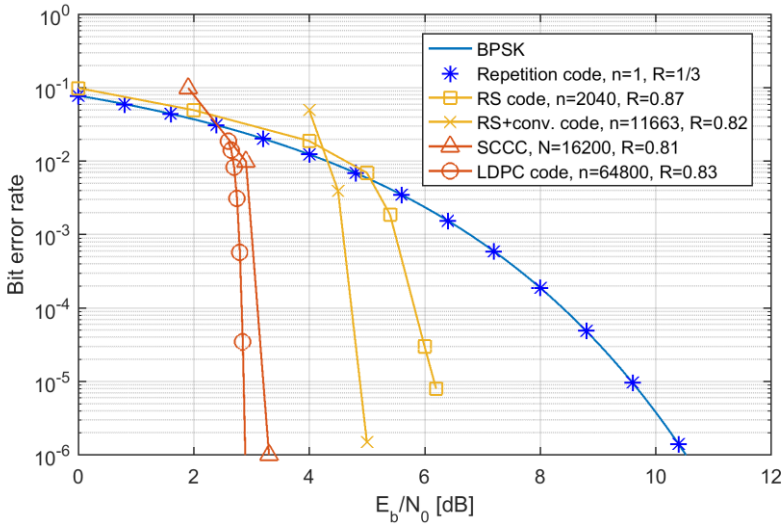

Figure 12-7: Comparison of different FEC schemes in terms of BER versus E_b/N_0 for a binary input AWGN channel. Additionally the bit error probability for uncoded BPSK is shown.

In Figure 12-7, bit error rate simulation results versus E_b/N_0—i.e. the energy per information bit to noise power spectral density ratio—for various CCSDS channel codes on an AWGN channel with BPSK are exemplified. One can observe from the figure that LDPC codes show the best performance among the considered channel codes. Notable gains in the order of a few dB is visible with respect to RS codes, concatenated RS, and convolutional code. Small gains in the order of a few tenths of dB are present with respect to SCCCs for the setup in the figure. From a bit-error rate performance point of view, LDPC and SCCCs are a natural choice, whenever complexity constraints are not stringent. As a complement, also the bit error rate versus E_b/N_0 of a repetition code with rate 1/3 is depicted under soft decoding. Observe that there is a gap of around 5.6 dB with respect to the LDPC at a bit error rate of 10^{-4}. Despite this gap, repetition codes might be a reasonable choice if decoding complexity is a bottleneck.

For correlated fading channels, the following additions to the channel coding options above can be made:

- **Long PHY interleaver** is usually placed after the channel encoder. Thereby code symbols of several codewords are interleaved among each other before modulation and transmission over the channel. In this setting 'long' means that the interleaver duration shall exceed the coherence time of the channel. This way after deinteleaving at the receiver side, errors introduced by the fading are spread over several code words. If the interleaver is chosen long enough, there is virtually no degraded code performance compared to an uncorrelated channel [50].
- **PKT code** is placed as an additional layer of error protection as a complement to the PHY code. To this end the user data is first portioned into packets and encoded by the PKT code where a code symbol in an entire packet. The data is then further encoded by a PHY code. The duration of a PKT codeword shall be longer than the channel coherence time.

Next various FEC schemes for data relay systems are discussed.

12.8.1 *Full Decoding on board of the relay*

Consider the U-R link. In fact, without complexity constraints on the relay the best solution in terms of bandwidth efficiency/error rate performance is the following: encode the data on the user side and decode it completely on board of the relay. This way, upon a proper choice of the modulation and coding scheme, nearly all errors are corrected on board of the relay and all redundancy data for U-R link is removed at the relay. Then, a further encoding of the recovered user data (not containing any redundancy) takes place to protect the data from errors on the R-G link. A modern channel code with high coding gain, such as an LDPC code would be the natural choice here. Soft decoding of a modern code on board of the relay is problematic from a complexity point of view, at least nowadays. Therefore, given stringent complexity constraints, simpler codes might be used paired with simple, preferably hard decoders. This yields performance losses that can be mitigated by considering alternative FEC schemes (see e.g., partial coding).

12.8.2 *Decoding on ground only*

As an alternative to full decoding on board of the relay, one may shift decoding complexity to the ground station where computation resources are plentiful. This scheme is called decoding on ground. On the one hand, this solution has the disadvantage that the bandwidth occupation increases, at least when the quality of the U-R link requires the use of medium/low code rates. For optical links, typically, power is plentiful, but fading events may require medium/lower code rates. On the other hand, decoding on ground only is a simple, low-complexity scheme with good performance and certain flexibility to modify the PHY FEC. In fact, among all considered schemes it put the lowest computational burden on the relay.

Due to technological constraints, often demodulation of the waveform at the relay takes place. This is followed by a modulation step. We call this type of relay systems semi-transparent. To exploit the full capabilities of modern codes and their soft iterative decoders (on ground), they need to have access to soft channel information. Consequently, soft demodulation of the U-R link signal at the relay is desirable. Denote by 2^q the number of quantization levels of the values at the demodulator output, i.e. each value is represented by q bits. After soft demodulation at the relay there is an increase of data rate by factor q. This implies that q times more bandwidth and power (aggregated) are required to transmit soft information after demodulation. A special case consist for $q = 1$. Hard demodulation at the relay can be done in order to improve the bandwidth efficiency on the R-G link and to reduce complexity at the relay. Usually, the use of hard demodulators is paired with a performance loss more than 2 dB compared to soft demodulation (see Figure 12-8). However, in the current setup the required bandwidth is reduced by a factor of q with respect to soft-demodulation and so does the required power (since only one and not q bits per demodulated code symbol need to be transmitted). Therefore, decoding on ground only with $q = 1$ is the preferred option.

There exist several flavors of decoding on ground only:

- **Two step encoding**: One may perform encoding at the user side to protect the data only from errors on the U-R link. Then, a second encoding step at

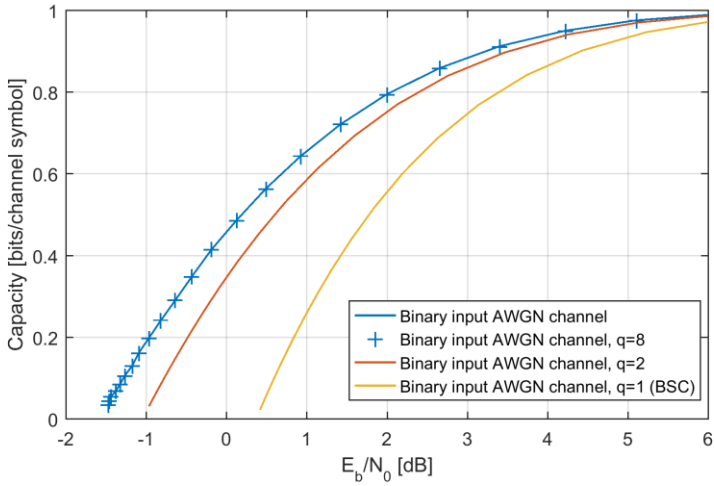

Figure 12-8: Channel capacity versus E_b/N_0 for binary-input AWGN channel with different quantization levels at the demodulator.

the relay takes place adding additional complexity (and reducing flexibility of the scheme). Let us denote by R_{ur} the code rate for the U-R link and by R_{rg} the code rate for the R-G link. The number of quantization levels is chosen to be $q = 1$. To transmit the k_{ur} bits, the U-R link needs to carry $k_{ur} \cdot 1/R_{ur}$ bits. After re-encoding on board of the relay, the R-G link needs to carry $k_{ur} \cdot 1/R_{ur} \cdot 1/R_{rg}$ bits. By contrast, when decoding on board of the satellite is allowed, the amount of bits is at most $k_{ur} \cdot 1/R_{rg}$ for the R-G link. This means a factor of $1/R_{ur}$ increase in required data rate (bandwidth) w.r.t. decoding at the relay.

- **<u>One step encoding</u>**: Another alternative is to perform encoding only at the user with a rate R_{ug} in order to protect the data against impairments on both U-R and R-G links. Then, no encoding at the relay needs to be done. We have that $\min(R_{ur}, R_{rg}) \geq R_{ug} \geq R_{ur}R_{rg}$. The semi-transparent relay performs demodulation and modulation. As sketched previously hard demodulation is the better choice from bandwidth/power consumption/complexity point of view. To transmit k_{ur} bits, now on both links $k_{ur} \cdot 1/R_{ug}$ bits need to be sent. For the same performance, higher bandwidth is required compared to decoding on board of the satellite. This option is a good choice when both communication channels allow high rate codes, i.e., when $R_{ur} \cdot R_{rg}$ is close to one or when bandwidth is plentiful.

Decoding on ground may not be the best choice in terms of bandwidth usage (or power usage for a fixed bandwidth). It is the most commonly employed scheme for relaying since it is flexible, highly performant and simple, i.e., it requires least processing capabilities on board of the relay.

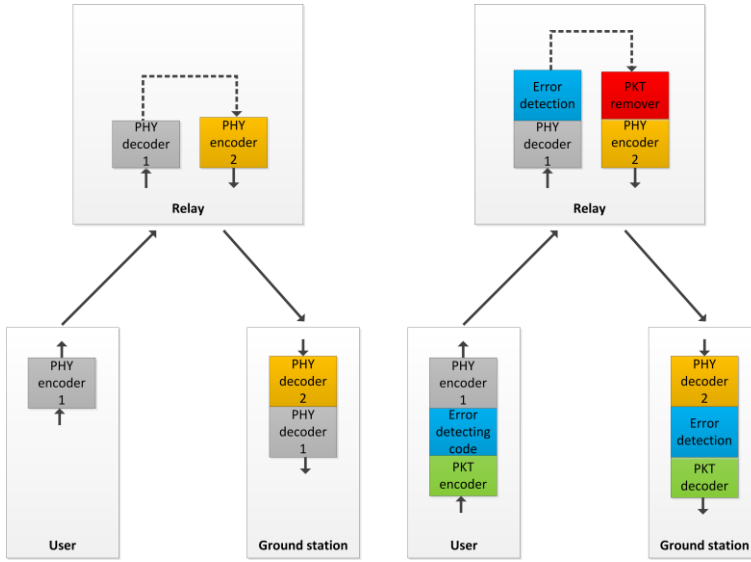

(a) (b)

Figure 12-9: General block diagram for (a) partial decoding scheme and (b) layered FEC scheme.

12.8.3 *Partial decoding scheme*

There exist several options for partial decoding. The main idea is to decode parts of the data at the relay using simple codes and decoders and to decode the rest on ground where more computational power is available. This way some errors might be directly corrected at the relay and unnecessary redundancy on the R-G link is avoided.

One may consider the following approach. At the user side, encoding takes place and the data is transmitted to the relay, where a first low-complexity decoding attempt is done. If decoding is successful, the redundancy added at the user side can be removed and the user data is forwarded to the encoder at the relay. If decoding is not successful, the entire erroneous codeword is forwarded to the encoder. Additional redundancy is added at the encoder and the data is forwarded to ground for decoding. If decoding on board succeeds, this scheme is similar to decoding on board of the relay as sketched before in terms of bandwidth constraints. If decoding does not succeed, the scheme is similar to decoding on ground only as sketched before. Clearly, the success of decoding on board of the relay is strongly related to the U-R link quality and the complexity limitations of the code/decoding algorithm. The setup is sketched in Figure 12-9(a).

Candidates for the PHY codes are for instance:

- **Low-memory convolutional codes with interleaving**. Here, convolutional codes with different memory can be considered, with coding gains with respect to the repetition code ranging from 4 dB (for the memory-2, rate ½ case) up to 7 dB (for the memory-6 case) under soft decision decoding.
- **Algebraic codes**, such as BCH codes (or RS codes). Efficient syndrome decoders based on look-up tables available and are e.g. used in terrestrial fiber optical communications for 100 Gbps links [51].

- **Concatenated schemes**. Concatenations of the above codes may yield a more powerful channel code. An example are BCH product codes as also used in terrestrial fiber optical communications [51] whose component codes might decoded at the relay, while (upon decoding failure at the relay) the product code is decoded on ground. Modern codes, such as LDPC or turbo codes also belong to the class of concatenated schemes [52][53]. Similarly, their component codes might be decoded at the relay (eventually using simple decoders), while the concatenated scheme is decoded on ground.

12.8.4 *Layered coding scheme*

A promising alternative in case of U-R (fading) links lies in the use of an additional PKT code. To this end, user data is split into K packets, each of them having L bits, and encoded by means of a PKT code yielding N packets, each of them having L bits. Each packet is further subject to an error detection mechanism (usually a CRC code or inherent error detection capability of the PHY decoder) in order to ensure its integrity after transmission. The packets are forwarded to lower layers. At PHY, usually a simple error correcting code is additionally used to protect the packets against sporadic bit errors due to noise, since a single bit error may corrupt an entire packet. The aim of using a PKT level code is to protect the data against sequences of errors introduced by the (correlated) communication channel.

After transmission on the U-R link, PHY decoding at the relay takes place to correct sporadic bit errors. Note that the PHY code is a simple code here, which can be tailored to the complexity limitation of the relay. In a next step, error detection takes place to check the integrity of all packets. All corrupted packets are discarded at the relay.

In order to spare bandwidth on the R-G link further packets at the relay can be discarded by a packet remover as follows. Denote by K' the number of correctly received packets at the relay. $K \leq K'$ is a necessary condition for successful decoding. For many codes, $K \leq K'$ is not sufficient to ensure decoding success. Therefore, let us require $K + \Delta \leq K'$, where Δ is a design parameter (also referred to as overhead) that is usually much smaller than K (e.g., in the order of a few percent of K). Else, decoding will fail with a high probability and one may discard all packets already at the relay. Assume that at the relay K' packets are correctly received. Then, a packet remover at the satellite discards packets until only $K + \Delta$ packets remain. The choice of the overhead gives a tradeoff between the code performance and bandwidth occupation on the R-G link.

After the packet remover, no decoding of the PKT code takes place at the relay. Instead, the remaining $K + \Delta$ packets are forwarded to lower layers, encoded again and transmitted over the R-G link. On ground, decoding of the code for the R-G link takes place. Then, again, error detection for each of the packets takes place. Finally, a PKT decoder attempts to correct the missing packets. The setup is sketched in Figure 12-9(b).

An advantage of the layered scheme lies in the fact that on board of relay no complex decoding operations take place. Only PHY decoding of a simple code needs to be done, followed by an error detection and packet removal step. The code used on PHY can be an algebraic code or a low memory convolutional code. Its purpose is to correct sporadic bit errors. Another advantage of the layered scheme is that the relay forwards only $K + \Delta$ packets to the lower layers, where K is the

number of information packets. For sake of comparison with the former schemes assume that $K \cdot L = k_{ur}$. To transmit a file of k_{ur} bits one has to send $(K + \Delta) \cdot L \cdot 1/R_{rg} = (k_{ur} + \Delta \cdot L) \cdot 1/R_{rg}$ bits on the user link. The parameter Δ is chosen to be a small fraction of K, typically in the order of a few percent.

Layered coding can be seen as a special case of partial decoding. Both schemes may implement a similar PHY code, complemented by a PKT code for layered decoding. While at the relay a low complex decoding attempt of the PHY code is done, on ground the PKT layer code is decoded in order to resolve residual errors on the U-R link. We point out that PKT level codes perform best on correlated communication channels. They work well if the PKT codeword duration is much longer than the coherence time of the channel.

12.8.5 *Interleaving options*

12.8.5.1 *Long PHY interleaver*

A typical strategy for correlated channels is the employment of long PHY interleavers. These interleavers spread over a multitude of code words. The goal is to let every codeword experience good and bad channel states. In this way, the number of errors in every codeword shall be similar after deinterleaving. Upon a proper choice of the code parameters, the number of errors in a codeword shall not exceed its error correcting capabilities and successful decoding is possible. On the contrary, without interleaving some code words would contain too many errors others maybe none. For a given date rate D, the length of the interleaver (interleaver depth d) is usually chosen such that d/D is much larger than the coherence time t of the channel. More formally $d = \mathrm{D} \cdot t \cdot c$, where $c \gg 1$. The value of c determines the code performance and needs to be carefully chosen for the targeted communication channel.

To assess the effect of the interleaver, consider performance of a rate 2/3 LDPC code of length 64800 on a lognormal block-fading channel with AWGN assuming BPSK. For the lognormal fading, let us choose the parameter $s = 0.5$ (standard deviation of the underlying Gaussian process). Further, choose m (mean of the underlying Gaussian process) such that the average power of the lognormal process is one.

The block-fading channel is implemented as follows. Based on a Markov process with average state duration $1/p_{ij}$ a channel state is selected. Each channel state is associated to a fading amplitude, sampled from a lognormal distribution. For the experiments different $1/p_{ij}$ were considered, where high values of $1/p_{ij}$ mimic a strongly correlated communication channel. The results are summarized in Figure 12-10.

In Figure 12-10 the curve with $1/p_{ij} = 1$ represents the frame error rate (FER) versus Eb/N0 for a rate-2/3 LDPC code of length $n = 64800$ symbols on a lognormal fading channel with no correlation. Significant losses in performance are visible if $1/p_{ij}$ is comparable to the codeword length n, i.e. for $1/p_{ij} = 64800$. This is owing to the fact that code symbols in a codeword often experience similar level of fading and the channel code is not capable of compensating for it. For $1/p_{ij} = n/100 = 648$ the loss compared to the uncorrelated case ($1/p_{ij} = 1$) is within 1.4 dB at a frame error rate of 10^{-2}. These observations suggest that for the example lognormal fading channel the interleaver depth shall be at least 100 times

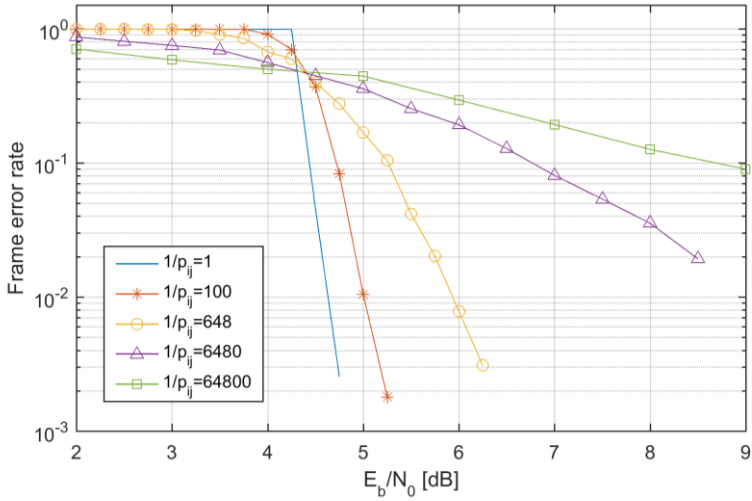

Figure 12-10: FER versus Eb/N0 of an (64800, 43200) LDPC code on a lognormal block fading channel for different average state durations.

larger than the channel coherence time times the data rate to avoid significant losses in performance.

Regarding the interleaver dimensioning the procedure is as follows:

- Determine the channel coherence time t and the required data rate D.
- Fix a value of c, based on simulations and/or constraints on available memory and/or delay constraints.
- Compute the interleaver depth $d = \mathrm{D} \cdot t \cdot c$.

12.8.5.2 *PKT code with interleaved code symbols (packets)*

Whenever PKT codes are used, the length of a PKT code word has to be chosen such that $NL/R_{PHY} = c \cdot \mathrm{D} \cdot t_{ur}$, where L denotes the packet size in bits, c a constant usually larger than one, D the data rate, t_{ur} the coherence time of the U-R link and R_{PHY} the code rate of the PHY code on the U-R link. The constraints here are as for the long PHY interleaver. In case of structured LDPC PKT codes on correlated channels, it is required that the code symbols (packets) are interleaved among each other before transmission to avoid performance losses.

12.8.6 *Comparison of coding schemes*

Consider a simplified setup, both for layered coding on board of the satellite. The R-G link is assumed ideal. This assumption can be justified if the PHY code—i.e. orange block in Figure 12-9(b)—is dimensioned in both cases such that it can correct quasi all error events on the R-G link. For the U-R link, consider a block lognormal fading channel with Gaussian noise and BPSK modulation. The mean state duration $1/p_{ij}$ was set to 64800 BPSK modulated channel symbols, while the parameter s of the lognormal distribution[4] was varied from 0.5 (considerable fading) to 0.015 (quasi AWGN channel). The following is analyzed:

[4] As before s is the standard deviation of the underlying Gaussian process.

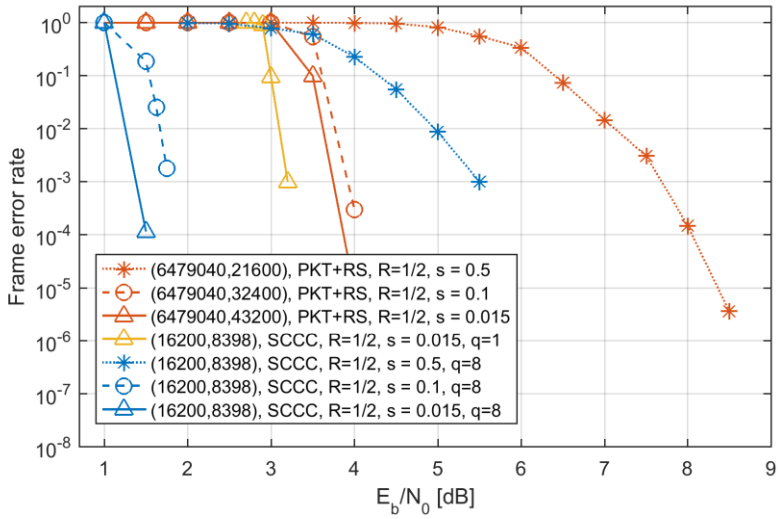

Figure 12-11: Comparison of layered coding and decoding on board of the satellite.

- **Layered coding (i.e., partial decoding complemented by a PKT code)**. Here a RS PHY code complemented by a maximum distance separable packet level code. The length of the RS-encoded PKT codeword was chosen to be approximately 6480000 bits with an overall rate of ½.
- **Full decoding on board of the satellite**. Assume a SCCC with rate 1/2 that is interleaved with a long PHY interleaver of length 6480000 symbols.

Further, at the semi-transparent satellite demodulation is done with q bits per bit reliability, with $q = 1$ or $q = 8$ for the SCCC scheme, while for layered coding always hard demodulation is done.

Figure 12-11 shows frame error rate performances of both schemes. Note that if for demodulation with $q = 8$ (quantized soft demodulator) of the SCCC coded modulation symbols there is a gain of around 2 to 2.4 dB w.r.t. the layered coding (at the price of a q times higher data rate on the R-G link). If q is chosen to be one (hard demodulator) the gain is less than 0.5 dB (magenta curve).

The results in Figure 12-11 suggest layered coding is a suitable option. In fact, assuming hard demodulation at the satellite, it provides similar performance (0.5 dB gap) to the best decoding strategy, full decoding at the relay, but with much lower complexity burden at the relay, while having similar spectral efficiency on both links. Note that (quantized) soft demodulation on board of the relay is often not desired. In particular, consider decoding on ground only: as discussed in Section 12.8.2, for $q > 1$ the data rate/bandwidth requirements are increased, but also the overall power requirements (since q symbols instead of one symbol need to be transmitted). This is clearly not desirable.

12.9 Summary

The analysis presented gives a general overview on different aspects for the communication chain in a relay-based system for high-speed data rates. The user sends its data down to Earth through a GEO satellite, and therefore there are two main links, namely the U-R and R-G links. A distinction of the user has been made, where either LEO satellites or UAVs have been considered. In case of the LEO platform user a small—e.g. CubeSat—and a large satellite have been taken into account. A channel model has been defined assuming that transmission through the U-R and R-G links is done optically. Special attention was taken into modeling the effects of the pointing errors, due platform micro-vibrations, for the user terminal, and dimensioning of the corresponding link has been accordingly. Next, based on the channel model, link budget calculations were performed in order to give an idea of the possibilities of future ultra-high-speed data relay systems. In addition, a receiver sensitivity analysis was done, based on extrapolation of previously reported experiments on the sensitivities for uncoded transmission. From this, possibly achievable maximum data rates were estimated for each link in the relay scenarios considered here, taking into account whether the receiver is set to work with direct or coherent detection.

Code design for relay systems depends on several constraints. Under strong complexity constraints on the relay and high powers on the U-R link (thus high code rates) decoding on ground only is the preferred option. Whenever the U-R link requires the use of a medium/low rate code, partial coding schemes and layered schemes are a good choice. For correlated fading channels, layered coding schemes exploit their full capabilities. If complexity constraints on the relay are not stringent, full decoding at the relay is the best choice.

12.10 Abbreviations

AO	Adaptive Optics
AWGN	Additive White Gaussian Noise
BCH	Bose-Chaudhuri-Hocquenghem
BER	Bit Error Rate
BPSK	Binary Phase-Shift Keying
CC	Convolutional Codes
CCSDS	Consultative Committee for Space Data Systems
CPA	Coarse Pointing Assembly
CWDM	Coarse Wavelength Division Multiplexing
DPSK	Differential Phase-Shift Keying
DWDM	Dense Wavelength Division Multiplexing
EDFA	Erbium-doped Fiber Amplifier
ESA	European Space Agency
FEC	Forward Error Correction
FER	Frame Error Rate

Gbit/s, Gbps	Gigabits per Second
GEO	Geostationary Equatorial Orbit
LCT	Laser Communications Terminal
LDPC	Low-Density Parity Check
LEO	Low Earth Orbit
LO	Local Oscillator
LPF	Low Pass Filter
L-R	Leo to Relay
Mbit/s, Mbps	Megabits per Second
NEP	Noise Equivalent Power
OGS	Optical ground station
OOK	On-Off Keying
OPLL	Optical Phase Locked Loop
PDF	Probability Density Function
PHY	Physical
PKT	Packet
PPM	Pulse Position Modulation
PSD	Power Spectral Density
RF	Radiofrequency
R-G	Relay to Ground
RS	Reed-Solomon
Rx	Receiver
SCCC	Serial Concatenated Convolutional Codes
SI	Scintillation Index
SMF	Single Mode Fiber
SNR	Signal-to-noise ratio
Tx	Transmitter
UAV	Unmanned aerial vehicle
U-R	User to Relay
WDM	Wavelength Division Multiplexing
X-R	UAV to Relay

References

[1] D. C. Troendle, C. Rochow, K. Saucke, N. Hoepcke, P. M. Pimentel, F. F. Heine, R. Meyer, M. Lutzer, and E. Benzi, “Alphasat TDP1 Three years optical GEO data relay operations,” in *34th AIAA International Communications Satellite Systems Conference*, 2016, pp. 2016–5700.

[2] M. Agnew, L. Renouard, and A. Hegyi, "EDRS-SpaceDataHighway: Near-real-time data relay services for LEO satellites and HAPs," in *30th AIAA International Communications Satellite System Conference, ICSCC*, 2012.

[3] Y. Koyama, M. Toyoshima, Y. Takayama, H. Takenaka, K. Shiratama, I. Mase, and O. Kawamoto, "SOTA: Small Optical Transponder for micro-satellite," in *Space Optical Systems and Applications (ICSOS), 2011 International Conference on*, 2011, pp. 97–101.

[4] G. D. Fletcher, T. R. Hicks, and B. Laurent, "The SILEX optical interorbit link experiment," *Electronics & Communication Engineering Journal*, vol. 3, no. 6, pp. 273–279, 1991.

[5] A. Alonso, M. Reyes, and Z. Sodnik, "Performance of satellite-to-ground communications link between ARTEMIS and the Optical Ground Station," in *Optics in Atmospheric Propagation and Adaptive Systems VII*, 2004, vol. 5572, no. 1, pp. 372–383.

[6] Y. Takayama, T. Jono, Y. Koyama, N. Kura, K. Shiratama, B. Demelenne, Z. Sodnik, A. Bird, and K. Arai, "Observation of atmospheric influence on OICETS inter-orbit laser communication demonstrations," in *Free-Space Laser Communications VII*, 2007, vol. 6709, no. 1, p. 67091B.

[7] M. Gregory, F. Heine, H. Kämpfner, R. Meyer, R. Fields, and C. Lunde, "Tesat laser communication terminal performance results on 5.6 gbit coherent inter satellite and satellite to ground links," in *International Conference on Space Optics ICSO 2010*, 2010.

[8] Z. Sodnik, B. Furch, and H. Lutz, "Optical Intersatellite Communication," *Selected Topics in Quantum Electronics, IEEE Journal of*, vol. 16, no. 5, pp. 1051–1057, 2010.

[9] G. Muehlnikel, H. Kämpfner, F. Heine, H. Zech, D. Troendle, R. Meyer, and S. Philipp-May, "The Alphasat GEO Laser Communication Terminal Flight Acceptance Tests," in *Proc. International Conference on Space Optical Systems and Applications (ICSOS)*, 2012.

[10] D. Giggenbach, P. Becker, R. Mata-Calvo, C. Fuchs, Z. Sodnik, and I. Zayer, "Lunar Optical Communications Link (LOCL): Measurements of Received Power Fluctuations and Wavefront Quality," in *Proc. International Conference on Space Optical Systems and Applications (ICSOS)*, 2014.

[11] Z. Sodnik, H. Smit, M. Sans, D. Giggenbach, P. Becker, R. Mata-Calvo, C. Fuchs, I. Zayer, M. Lanucara, K.-J. Schulz, J. Widmer, F. Arnold, M. Mosberger, A. Alonso, and I. Montilla, "Results from a Lunar Laser Communication Experiment between NASA's LADEE Satellite and ESA's Optical Ground Station," in *Proc. International Conference on Space Optical Systems and Applications (ICSOS)*, 2014.

[12] D. M. Boroson, B. S. Robinson, D. V. Murphy, D. A. Burianek, F. Khatri, J. M. Kovalik, Z. Sodnik, and D. M. Cornwell, "Overview and results of the Lunar laser Communication Demonstration," in *Free-Space Laser Communication and Atmospheric Propagation XXVI*, 2014, vol. 8971, p. 89710S.

[13] B. L. Edwards, D. Israel, K. Wilson, J. Moores, and A. Fletcher, "Overview of the laser communications relay demonstration project," in *Proceedings of SpaceOps*, 2012, vol. 1261897.

[14] B. Friedrichs, "Data processing for broadband relay satellite networks–digital architecture and performance evaluation," in *Proc. Int. Commun. Satell. Syst. Conf.*, 2013.

[15] L. C. Andrews and R. L. Philips, *Laser Beam Propagation through Random Media*, 2nd ed. Bellingham: SPIE Press, 2005.

[16] N. Perlot and D. Fritzsche, "Aperture-Averaging – Theory and Measurements," in *Free-Space Laser Communication Technologies XVI*, 2004, vol. 5338, pp. 233–242.

[17] F. Vetelino, "Fade statistics for a lasercom system and the joint PDF of a Gamma-Gamma distributed irradiance and its time derivative," Department of Mathematics, University of Central Florida, 2006.

[18] B. Epple, "Simplified Channel Model for Simulation of Free-Space Optical Communications," *J. Opt. Commun. Netw.*, vol. 2, no. 5, pp. 293–304, 2010.

[19] J.-M. Conan, G. Rousset, and P.-Y. Madec, "Wave-front temporal spectra in high-resolution imaging through turbulence," *JOSA A*, vol. 12, no. 7, pp. 1559–1570, 1995.

[20] G. A. Tyler, "Bandwidth considerations for tracking through turbulence," *J. Opt. Soc. Am. A*, vol. 11, no. 1, pp. 358–367, 1994.

[21] J. Horwath, F. David, M. K. Knapek., and N. Perlot, "Coherent Transmission Feasibility Analysis," in *Free-Space Laser Communication Technologies XVII*, 2005, vol. 5712, pp. 13–23.

[22] S. Schaefer, M. Gregory, and W. Rosenkranz, "Coherent receiver design based on digital signal processing in optical high-speed intersatellite links with M-phase-shift keying," *Optical Engineering*, vol. 55, no. 11, p. 111614, 2016.

[23] D. Giggenbach and H. Henniger, "Fading-loss assessment in atmospheric freespace optical communication links with on-off keying," *Opt. Eng.*, vol. 47, no. 4, p. 046001, 2008.

[24] K. Kiasaleh, "On the probability density function of signal intensity in free-space optical communications systems impaired by pointing jitter and turbulence," *Opt. Eng.*, vol. 33, no. 11, pp. 3748–3757, 1994.

[25] M. Toyoshima, Y. Takayama, H. Kunimori, T. Jono, and S. Yamakawa, "In-orbit measurements of spacecraft microvibrations for satellite laser communication links," *Optical Engineering*, vol. 49, no. 8, pp. 83604–83604, 2010.

[26] M. E. Wittig, L. Van Holtz, D. E. L. Tunbridge, and H. C. Vermeulen, "In-orbit measurements of microaccelerations of ESA's communication satellite OLYMPUS," in *Free-Space Laser Communication Technologies II*, 1990, vol. 1218, pp. 205–214.

[27] J. Horwath and C. Fuchs, "Aircraft to ground unidirectional laser-communications terminal for high-resolution sensors," in *Lasers and Applications in Science and Engineering*, 2009, vol. 7199, pp. 7199–9.

[28] R. Nelson, T. Ebben, and R. Marshalek, "Experimental verification of the pointing error distribution of an optical intersatellite link," in *1988 Los Angeles Symposium–OE/LASE'88*, 1988, pp. 132–142.

[29] G. Planche and V. Chorvalli, "SILEX in-orbit performances," in *5th International Conference on Space Optics*, 2004, vol. 554, pp. 403–410.

[30] M. Toyoshima, "Near-earth laser communications," H. Hemmati, Ed. CRC press, 2009.

[31] F. David, D. Giggenbach, H. Henniger, J. Horwath, R. Landrock, and N. Perlot, "Design considerations for optical inter-HAP links," in *Proceedings ICSSC, 22nd AIAA International Communications Satellite Systems Conference & Exhibit, Monterey, CA*, 2004.

[32] R. G. Marshalek, "Near-Earth Laser Communications," H. Hemmati, Ed. Boca Raton, FL: CRC Press, 2009, p. 59.
[33] F. Fidler, "Optical communications for high-altitude platforms," Technischen Universitaet Wien, Wien, 2007.
[34] D. Giggenbach, R. Purvinskis, M. Werner, and M. Holzbock, "Stratospheric optical inter-platform links for high altitude platforms," in *Proceedings of the 20th International Communications Satellite Systems Conference, Montreal*, 2002.
[35] H. Takenaka, M. Toyoshima, and Y. Takayama, "Experimental verification of fiber-coupling efficiency for satellite-to-ground atmospheric laser downlinks," *Opt. Express*, vol. 20, no. 4, pp. 15301–15308, 2012.
[36] Y. Dikmelik and F. M. Davidson, "Fiber-coupling efficiency for free-space optical communication through atmospheric turbulence," *Applied Optics*, vol. 44, no. 23, pp. 4946–4952, 2005.
[37] R. J. Noll, "Zernike polynomials and atmospheric turbulence," *J. Opt. Soc. Am.*, vol. 66, no. 3, pp. 207–211, 1976.
[38] M. P. Cagigal and V. F. Canales, "Generalized Fried parameter after adaptive optics partial wave-front compensation," *J. Opt. Soc. Am. A*, vol. 17, no. 5, pp. 903–909, 2000.
[39] R. D. Hudson, *Infrared System Engineering*. New York: John Wiley & Sons, 1969.
[40] L. N. Binh, *Optical fiber communication systems with Matlab and Simulink models; 2nd ed.* Hoboken, NJ: CRC Press, 2014.
[41] P. J. Winzer, A. Kalmar, and W. R. Leeb, "Role of amplified spontaneous emission in optical free-space communication links with optical amplification: impact on isolation and data transmission and utilization for pointing, acquisition, and tracking," in *Proc. SPIE*, 1999, vol. 3615, pp. 134–141.
[42] M. Seimetz, *High-order modulation for optical fiber transmission*, vol. 143. Springer, 2009.
[43] B. Moision, J. Wu, and S. Shambayati, "An optical communications link design tool for long-term mission planning for deep-space missions," in *Aerospace Conference, 2012 IEEE*, 2012, pp. 1–12.
[44] D. O. Caplan, "Laser communication transmitter and receiver design," *Journal of Optical and Fiber Communications Reports*, vol. 4, no. 4–5, pp. 225–362, 2007.
[45] M. Peleg and S. Shamai, "On the capacity of the blockwise incoherent MPSK channel," *IEEE transactions on Communications*, vol. 46, no. 5, pp. 603–609, 1998.
[46] Huawei, "Polar Codes: A 5G enabling FEC scheme," *HIRP Journal*, vol. 1, no. 1, pp. 2044–2047, Jun. 2015.
[47] "Flexible Advanced Coding and Modulation Scheme for High Rate Telemetry Applications," no. 131.2.B.1. Consulative Committee for Space Data Systems (CCSDS), Washington DC, Mar-2012.
[48] *Digital Video Broadcasting (DVB); Second Generation Framing Structure, Channel Coding and Modulation Systems for Broadcasting, Interactive Services, News Gathering and Other Broadband Satellite Applications (DVB-S2)*. ETSI, 2009.
[49] A. K. Majumdar, *Advanced Free Space Optics (FSO)*. New York, NY, USA: Springer, 2015.

[50] S. J. Zhang X. Blow K. Fowler Liu, "Low-complexity decoding for non-binary LDPC codes in high order fields," *IET Communications*, vol. 11, no. 13, pp. 2042–2048, Nov. 2017.

[51] B. Smith, A. Farhood, A. Hunt, F. R. Kschischang, and J. Lodge, "Staircase Codes: FEC for 100 Gb/s OTN," *Journal of Lightwave Technology*, vol. 30, no. 1, pp. 110–117, Jan. 2012.

[52] R. Gallager, *Low-density parity-check codes*. Cambridge, MA, USA: MIT Press, 1963.

[53] C. Berrou, A. Glavieux, and P. Thitimajshima, "Near Shannon limit error-correcting coding and decoding: Turbo-codes," in *Proc. IEEE Int. Conf. Commun. (ICC)*, 1993.